Original

Yigit, C.; Heyda, J.; Ballauff, M.; Dzubiella, J.:

Like-charged protein-polyelectrolyte complexation driven by charge patches

In: The Journal of Chemical Physics (2015) AIP

DOI: 10.1063/1.4928078

Like-charged protein-polyelectrolyte complexation driven by charge patches

Cemil Yigit,[1,2,3] Jan Heyda,[4] Matthias Ballauff,[1,2,3] and Joachim Dzubiella[1,2,3,a)]
[1]*Soft Matter and Functional Materials, Helmholtz-Zentrum Berlin, 14109 Berlin, Germany*
[2]*Helmholtz Virtual Institute "Multifunctional Biomaterials for Medicine," 14513 Teltow, Germany*
[3]*Institut für Physik, Humboldt-Universität zu Berlin, 12489 Berlin, Germany*
[4]*Department of Physical Chemistry, University of Chemistry and Technology, Prague, 166 28 Praha 6, Czech Republic*

(Received 10 March 2015; accepted 1 June 2015; published online 12 August 2015)

We study the pair complexation of a single, highly charged polyelectrolyte (PE) chain (of 25 or 50 monomers) with like-charged patchy protein models (CPPMs) by means of implicit-solvent, explicit-salt Langevin dynamics computer simulations. Our previously introduced set of CPPMs embraces well-defined zero-, one-, and two-patched spherical globules each of the same net charge and (nanometer) size with mono- and multipole moments comparable to those of globular proteins with similar size. We observe large binding affinities between the CPPM and the like-charged PE in the tens of the thermal energy, k_BT, that are favored by decreasing salt concentration and increasing charge of the patch(es). Our systematic analysis shows a clear correlation between the distance-resolved potentials of mean force, the number of ions released from the PE, and CPPM orientation effects. In particular, we find a novel two-site binding behavior for PEs in the case of two-patched CPPMs, where intermediate metastable complex structures are formed. In order to describe the salt-dependence of the binding affinity for mainly dipolar (one-patched) CPPMs, we introduce a combined counterion-release/Debye-Hückel model that quantitatively captures the essential physics of electrostatic complexation in our systems. © *2015 AIP Publishing LLC.* [http://dx.doi.org/10.1063/1.4928078]

I. INTRODUCTION

Protein-polyelectrolyte (PE) complexes are of great importance in soft matter science and industry due to their functional incorporation into applications in bioengineering, pharmaceutics, cosmetics, or food technology.[1–4] For example, proteins used as drug carrier systems can be coated with PEs to avoid toxic reactions in the host environment.[5] Another example is that PEs are also employed to stabilize or destabilize proteins in solution.[6,7] The interaction between proteins and PEs depends on several chemical and physical factors, i.e., the pH, ionic strength, protein surface charge distributions, and the PE charge, length, and stiffness.[8,9] As a consequence, protein-PE complexation is a highly intricate process with a large variety of resulting stable structures. Hence, to address the challenges in designing novel materials based on protein-PE complexes, the driving forces behind the association process have to be understood in more detail.

Besides experimental efforts,[8,9] various theoretical approaches[10–15] and computer simulation analyses[16–30] were introduced to explain the formation and structure of protein-PE complexes. Most of the theoretical investigations are focused on the interaction between a PE chain and *oppositely* charged macromolecules, driven essentially by the leading order monopole electrostatic attraction. However, several experimental studies have demonstrated complexation of polyanionic PEs to like-charged proteins, also called complexation "on the wrong side" because the PE binds to the protein at a pH above its isoelectric point.[31–34] Explanations to this on a first sight surprising result revolve around ionic correlations,[21,35,36] charge regulation,[25] or the existence of heterogeneous charge distributions, in particular charge patches.[15,24,31–33] For the latter, it has been argued that multipolar interactions,[15,37] such as charge-dipole attractions,[29] dominate at short distances over the monopole repulsion. The notion of the dominance of the short-ranged attraction interaction between globally neutral (or near-neutral) but electrostatically heterogeneous macroparticles has been discussed in particular by Wu *et al.*[37] In view of this dominance, attractive electrostatic forces between domains of opposite charges were predicted to outweigh repulsions between domains carrying charges of equal sign, playing an important role in processes like aggregation of polyampholytic proteins or polyelectrolyte adsorption.

In another line of reasoning,[38–40] mostly revolving around protein adsorption to PE brushes on the wrong side,[41–44] it was concluded that counterion-release (CR) mechanisms[45–49] ruled the complexation on the wrong side. Here, strongly "condensed" ions on the PE chain and possibly also on the protein patches are assumed to be released upon complexation accompanied by a large favorable increase of entropy. This was recently supported by a combination of titration experiments and explicit-ion simulations of the like-charge complexation of Human Serum Albumin (HSA) with a short PE chain.[30] However, a systematic quantification of the counterion-release

a)joachim.dzubiella@helmholtz-berlin.de

contributions to protein-PE binding affinities has not been attempted before, to the best of our knowledge. In particular, it is not clear if weakly curved charge patches contribute to the free energy in the sense that ions really condense on such geometries[50–52] and are released upon complexation, as, for instance, in the pair association of oppositely charged PE chains.[49,53] In addition, for a quantitative description of complexation of like-charged macromolecules, the counterion-release picture is somewhat incomplete since it does not account for the monopole repulsion between the associating partners.

The goal of the present work is to better understand the complexation between a highly charged PE chain and a like-charged globular protein, *driven by charge patchiness*. For this purpose, we employ our recently constructed set of charged patchy protein models (CPPMs) with well-defined patchiness and multipolarity as well as discrete surface charges[54] and investigate systematically the complexation using explicit-salt, implicit-solvent computer simulations. In this way, effects of multipolar attractions and ion-condensation effects can be evaluated and explored in great detail. We thus provide valuable insights into patchiness-governed CPPM-PE conformations as well as the effective (orientation-averaged) interaction between the PE and the CPPM, the number of 'condensed' ions on both molecules, and the mutual orientation along their centers of mass separation. We further provide a qualitative analysis of the salt-concentration dependence of the binding affinity of the PE at hand of the useful counterion-release concept, eventually combined with a simple Debye-Hückel (DH) model to consider screening effects. Our study and the provided simulation tools should be useful for a better rationalization of the effects of charge patchiness on PE-protein complexation with which an improved interpretation and guidance of experimental efforts shall be achievable.

II. METHODS

A. Charged patchy protein models

We have recently introduced spherical particle models for nanometer-sized globular proteins of well-defined patchiness and multipolarity, including the effects of charge discreteness, in the following called CPPMs.[54] Briefly, all CPPMs have a radius $R_P = 2$ nm. This is a size typical for small globular proteins such as lysozyme or lactoglobulin.[55] We have constructed CPPMs with one ($m = 1$) or two ($m = 2$) patches. In particle models with two patches, the patches are antipodally directed, that is, on the exact opposite sides. In order to assign a net charge Q_P to the patchy particle, we fixed the number of negatively and positively charged beads to be $N_n = 37$ and $N_p = 29$ in all CPPMs. Thus, the resulting net charge of the patchy particles is $Q_P = -8e$ for all CPPMs, comparable to net charges of proteins of similar size at physiological conditions. The N_n negative charges are homogeneously distributed on the surface outside of the positive patch. The remaining $N_p - m \cdot s$ positive charges are distributed in such a way that charged beads (positive or negative) are not immediately adjacent. Our CPPMs are denoted by P_s^m where m specifies the number of patches and s specifies the number of positively charged beads per patch.

Illustrative snapshots of the employed CPPMs are provided in Table I, together with a summary of the CPPM features, in particular, the dipole moments. In our models, we consider $m = 1, 2$ and $s = 8, 12, 16$ resulting in mean patch charge densities (per area) around 1–2 e/nm^2 stemming from a local assembly of a few amino acids separated from each other by a few Ångströms.[9,56] The dipole moments are in the range of 159–1633 D, cf. Table I, also comparable to proteins of this size. Lactoglobulin, for instance, has 730 D.[57] The quadrupolar moments of the CPPMs are given elsewhere.[54]

B. Polyelectrolyte

A single flexible PE is modeled in a coarse-grained fashion as a sequence of N_{mon} freely jointed beads. Each bead represents a monomer with a radius σ_{LJ} and an electric charge of one negative elementary charge e. Thus, the fraction of ionized monomers is $f_{\mathrm{mon}} = 1$. The PE monomers are connected by a harmonic bond potential with an equilibrium bond length $l = 0.4$ nm and a force constant $k = 4100$ kJ mol^{-1} nm^{-2}. The flexibility of the PE chain is ensured via a harmonic angle potential in which the angle between a triplet of monomers is $\phi = 120°$ and the force constant is $k_\phi = 418$ kJ mol^{-1} rad^{-2}. In our study, we consider relatively short PE chains with a number of monomers of $N_{\mathrm{mon}} = 25$ and $N_{\mathrm{mon}} = 50$ as used in related

TABLE I. Summary of our charged patchy protein models (CPPMs) denoted by P_s^m. The index m stands for the number of patches, while s denotes the number of positive charges on each patch. In the images of the CPPMs in the top row, the pink beads depict the negatively charged atoms, while turquoise beads depict the positively ones. Yellow and white atoms depict the same neutral atoms and are only distinguished here to better illustrate the patch region which roughly has an area of 3 nm^2. All CPPMs have a radius of $R_P = 2$ nm and a net charge of $Q_P = -8e$. The CPPMs carry individual dipole moments as also summarized in the table. The corresponding quadrupolar (tensorial) moments are provided elsewhere.[54]

	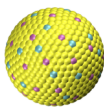	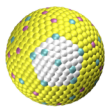	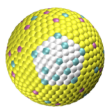	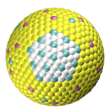	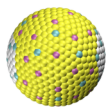	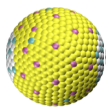
Label	P_0^0	P_8^1	P_{12}^1	P_{16}^1	P_8^2	P_{12}^2
Radius R_P (nm)	2	2	2	2	2	2
Patch area A_P (nm^2)	0	3	3	3	3 (×2)	3 (×2)
Total charge Q_P (e)	−8	−8	−8	−8	−8	−8
Dipole moment μ_P (D)	158.67	896.03	1328.71	1632.67	206.41	151.12

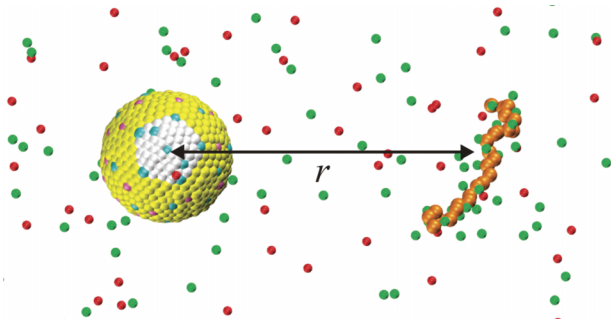

FIG. 1. Simulation snapshot of the CPPM P_8^1 (left) interacting with a coarse-grained 25meric PE chain (orange chain of pearls; right) in a center-to-center-distance r in explicit salt (free red and green beads) at 20 mM concentration.

experimental studies.[30,58–60] See also Fig. 1 for an example snapshot of a CPPM P_8^1 and a 25meric chain in 20 mM salt.

C. Simulation details

The simulation details are the same as in our preceding work where the CPPMs were introduced.[54] Briefly, the dynamics of each of the beads in our simulations is governed by Langevin's equation of motion,

$$m_i \frac{d^2 \boldsymbol{r}_i}{dt^2} = -m_i \xi_i \frac{d\boldsymbol{r}_i}{dt} + \boldsymbol{\nabla}_i U + \boldsymbol{R}_i(t), \tag{1}$$

where m_i and ξ_i are the mass and friction constant of the ith bead, respectively. U is the system potential energy and includes harmonic angular and bonded interactions between neighboring beads, and interatomic Lennard-Jones (LJ) between all non-neighboring beads. Coulomb interactions govern the electrostatic pair potential between all charged beads (including ions). The force $\boldsymbol{R}_i(t)$ is a Gaussian noise process and satisfies the fluctuation-dissipation theorem,

$$\langle \boldsymbol{R}_i(t) \cdot \boldsymbol{R}_j(t') \rangle = 2 m_i \xi_i k_B T \delta(t - t') \delta_{ij}. \tag{2}$$

The simulations are performed using the GROMACS 4.5.4 software package.[61] A leap-frog algorithm with a time step of 2 fs is used to integrate the equations of motion. A cubic box with side lengths of $L = 30$ nm is employed and periodically replicated to generate a quasi-infinite system in the canonical ensemble. The Langevin thermostat with $\xi_i = 0.5$ ps^{-1} holds the temperature at $T = 298$ K. Center of mass translation of the system is removed every 10 steps. The Particle-Mesh-Ewald[62] (PME) method is implemented to account for long-range electrostatics. The PME interaction is computed with a cutoff radius set to 1.2 nm to calculate the real-space interactions, while in the reciprocal space, a FFT grid of ~0.47 nm spacing is used with a cubic interpolation of fourth-order. This choice of parameters represented the best compromise between efficiency and accuracy where tests showed that PME errors were within the statistical fluctuations of the free energy calculations described below. The solvent is modeled as a continuous background medium (also within the CPPM) with a static dielectric constant $\epsilon_r = 78.44$ whereas the ions are explicitly considered. All particles (either a bead or an ion) have mass $m_i = 1$ amu, diameter $\sigma_{LJ} = 0.3$ nm, energy well $\epsilon_{LJ} = 0.1$ k_BT, and integer charges $q = 0, +1$ or $-1e$. The mass was chosen artificially low to enhance orientational fluctuations and sampling. Clearly, equilibrium properties, as investigated in this work, are not affected by any reasonable mass choices as long as the simulations are ergodic.

With the above specified settings, a pair of one CPPM and one PE in explicit salt were simulated for various CPPM types. The CPPM was position-restrained in the box center while still orientationally free. The PE was positioned initially at a distance of $r \sim 11$ nm with respect to their individual mass centers. Electroneutrality is ensured by adding the corresponding number of counterions. Additionally, monovalent salt with a concentration between $c_s = 10$ mM and 200 mM was added to the system. Because all ions were randomly placed initially, the system was relaxed for 100 ps to remove local contacts and afterwards equilibrated for 30 ns. An illustrative simulation snapshot is shown in Fig. 1.

D. PMF calculations from simulations

For calculating the potential of mean force (PMF) between a CPPM and the PE, we employed steered simulations using the pull code as provided by GROMACS.[61] Here, the center of mass of the PE is restrained in space by an external time-dependent force. This force is applied as a constraint, i.e., harmonic potential, and moved with a constant pulling velocity v_p to steer the particle in the prescribed direction.[63] After several test runs, the pulling rate $v_p = 0.1$ nm/ns was chosen which is small enough to warrant equilibrium sampling. The harmonic force constant $K = 2500$ kJ mol^{-1} nm^{-2}. The simulations were performed for ~90 ns. Given the pulling speed above, this simulation time is required to bring the two macromolecules from a separated state ($r \sim 11$ nm) to the fully complexed state ($r \sim 2$ nm). The standard deviation was calculated by standard block averages to specify the statistical error.

Output from the simulation is the total (nonequilibrium) mean force versus the distance coordinate. The friction force $F = -m\xi v_p$ was subtracted from this curve and averaged within a specific interval of discrete spacing Δr to obtain the equilibrium mean force. According to our simulation setup, the mean force was integrated backwards to get the PMF. Because the CPPM were constraint in space, the PMF has to be corrected for entropic effects[64–66] by

$$w(r) = w^{\mathrm{I}}(r) - (c - 1) \mathrm{k_B T} \ln(r), \tag{3}$$

where $w^{\mathrm{I}}(r)$ is the integrated mean force and $c = 3$ is the dimension of the constraint.

III. ANALYSIS

A. Mie potential (MP)

In order to describe the purely non-electrostatic interaction between a CPPM and a PE, we also consider the PMF between a completely neutral CPPM-PE pair as a reference model, where none of the atomic beads is charged. This PMF is thus created solely by a combination of the total van der Waals (vdW) attraction and Pauli repulsion that add up from the Lennard-Jones interactions between the individual beads as well as from the changes in PE chain configurational entropy

upon approach. For the description of this PMF, we employ a shifted MP of the form

$$U_{\mathrm{MP}}(r) = \frac{n}{n-m}\left(\frac{n}{m}\right)^{\frac{m}{n-m}} \cdot \epsilon^* \cdot \left[\left(\frac{\sigma^*}{r-2R_0}\right)^n - \left(\frac{\sigma^*}{r-2R_0}\right)^m\right], \quad (4)$$

where the exponents $n > m$ describe the steepness of the repulsive and attractive parts, respectively, and ϵ^* and σ^* are the depth and range of the attractive potential well, while r is the center-to-center separation. The potential is shifted by a distance R_0, where the repulsion diverges.

B. Patch orientation

The introduction of a patch vector provides a method to analyze the angular orientation of the patch between the mass centers of the CPPM and the PE in dependence of their center-to-center separation $\boldsymbol{r}$, as represented in Fig. 2. The patch vector $\boldsymbol{p}$ points from the particle center to the patch center and provides also a very good approximation of the dipole direction of the P_s^1 models. In our analysis, we computed the distance-resolved cosine of the angle $\theta(r)$ by

$$\cos[\theta(r)] = \left\langle \frac{\boldsymbol{p}\cdot\boldsymbol{r}}{|\boldsymbol{p}|\cdot|\boldsymbol{r}|}\right\rangle_r, \quad (5)$$

where we average $\langle..\rangle_r$ at a fixed distance r. The distance-dependent angular correlation of the patch vectors is calculated via the second Legendre polynomial $P_2(\cos[\theta])$ with $P_2(x) = (3x^2-1)/2$. In CPPMs with two patches, only one patch is used to calculate the orientation since the patches are antipodally directed.

C. Ion-condensation and counting

In order to count ions in the immediate vicinity of a molecular surface of arbitrary shape, a finite volume element over the surface is constructed. The volume element is made up from the superposition of spheres with a fixed radius $r_s = 0.4$ nm centered at each molecular bead S_i, being a bead corresponding either to a CPPM patch or the PE chain, respectively. Since the surface can be contorted, care is taken to the overlapping volumes to avoid double counting of ions. According to our definition, ions found in the volume element are *condensed* on the molecular surface and N_C denotes the number of condensed ions.

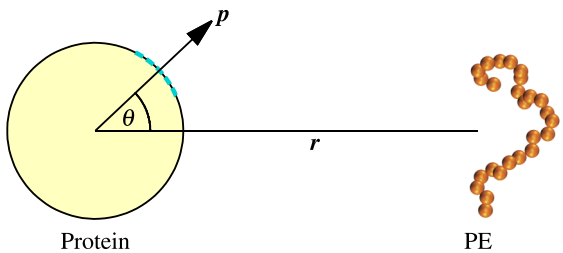

FIG. 2. A geometrical sketch of the patch orientation. The angular orientation θ is defined by the patch vector $\boldsymbol{p}$ and the distance vector $\boldsymbol{r}$ connecting the two centers of mass of both molecules.

D. Salt concentration dependence of the binding affinity

An important quantity in the complexation process is the binding affinity of the PE to the CPPM which in principle is an easily accessible number in experiments through the measurement of equilibrium constants.[8,9,30] Since we resolve the total PMF along the distance coordinate, the binding affinity can be naturally defined as the difference in free energy of the stable complex versus the separated reference state. Hence, the binding free energy can be written as

$$w_{min}(c_s) = w(r_{min}; c_s), \quad (6)$$

where r_{min} is the location of the global minimum of the PMF characterizing the stable complex. This binding affinity is in general a sum of vdW, PE chain entropy, and multipolar electrostatic contributions (including ionic entropy effects). However, the first two parts are at least one order of magnitude smaller than the electrostatic one for our systems and will therefore be neglected in our discussion. For the interpretation of the resulting salt concentration dependence of the electrostatic part, we compare our simulations to the classical counterion-release mechanism and complement it eventually to include screening effects by mapping our system onto a highly simplified model of an interacting charge-dipole system in the DH limit.

1. Counterion-release

The counterion-release concept goes back to the mean-field "Onsager-Manning-Oosawa" theories[45–48] that predict that counterion-condensation can occur on highly charged rod-like molecules or under some circumstances also on other macromolecular geometries.[50–52] Here, a fraction of the neutralizing counterions are tightly bound within a critical distance from the charged surface while the remaining, 'screening' ones are diluted away in the bulk. For instance, for rod-like molecules, such as an polyelectrolyte, the counterion condensation mechanism for monovalent salts is controlled by the Manning parameter,

$$\xi = z\lambda_B/l, \quad (7)$$

where we recall that $l = 0.4$ nm is the bond length (or inverse line charge density), $\lambda_B = e^2/(4\pi\epsilon_o\epsilon_r k_B T) = 0.71$ nm is the Bjerrum length for water at room temperature, and $z = 1$ the counterion valency. According to Onsager-Manning-Oosawa theory, counterion condensation occurs if $\xi > 1$, i.e., the Manning parameter exceeds unity. Theory predicts in the limit of vanishing salt that a fraction $x = 1 - 1/\xi$ of ions is then condensed on the PE in a highly dense state. That means that for a PE with N_{mon} monovalent charges xN_{mon} of them are on average neutralized by bound ions.

Record and Lohman utilized this fact to successfully explain salt concentration dependencies of the binding affinities of charged ligand–nucleic acid associations and predicted that[49]

$$\beta w_{min}(c_s) \propto N' \ln(c_s), \quad (8)$$

where N' reflects the number of strongly bound (and high density) ions released from the PE chains upon complexa-

tion. The physics behind Eq. (8) is simply understood by the fact that N' ions are released into bulk with a much lower salt concentrations upon complexation, leading to substantial gain of translational entropy of the ions. (Recall that Eq. (8) resembles the expression for the translational free energy of N' ideal gas particles.) We note that a clear distinction between "condensed" ions and densely bound "screening" ions is not always strictly possible at finite salt concentrations[67] and flexible chains. The approach of Record and Lohman described semi-quantitatively the complexation of pairs of short, highly charged PE chains, where ions are indeed confined in a well-defined fashion.[49]

For our analysis of the CPPM-PE complexation, we follow similar arguments that build up on the counterion-release concept and were originally introduced to rationalize the interaction between patchy, charged globular proteins and like-charged PE brushes.[44] Here, it was assumed that additionally to the N_+ counterions on the negative PE also N_- counterions on a highly charged positive patch on the protein are condensed for large separation distances between the molecules. Upon association, a certain number ΔN_- and ΔN_+ of ions are released. The change of the (total entropic) free energy for this process was argued to be

$$\begin{aligned}\beta w_{min}(c_s) &\sim \beta w_{\text{patch}} + \beta w_{\text{PE}} \\ &= \Delta N_- \ln\left[\frac{c_s}{c_{\text{patch}}}\right] + \Delta N_+ \ln\left[\frac{c_s}{c_{\text{PE}}}\right], \end{aligned} \tag{9}$$

where c_{patch} is the concentration of ions accumulated on the positive protein patch and c_{PE} is the concentration of "condensed" ions in the vicinity of the PE. We calculate $c_{\text{patch}} = N_-/V_{\text{patch}}$, where N_- is counted as described in Section III C and we assume that $V_{\text{patch}} = A_P d$ with a patch area of $A_P = 3$ nm^2 and the ionic layer thickness is $d = 0.4$ nm. This value on the order of the bead-bead interaction diameter is a reasonable choice to account for directly bound ions as can be seen from the density distribution of ions around the patches plotted in our previous work.[54] To determine $c_{\text{PE}} = N_+/V_{\text{PE}}$, we calculate the density distributions of ions around the individual monomers and found a weakly salt-dependent $c_{\text{PE}} \simeq 3.5 \pm 0.5$M in our concentration range from 10 to 200 mM.

2. A simple model to combine ionic release and screening effects

An obvious weakness of the counterion-release approach above is that it only captures the translational entropy contributions of the ions tightly condensed in the first layer of the CPPM and the PE. While this is justified for the PE, the picture is not so clear for ions condensing on the charge patch of a weakly curved spherical surface.[50–52] For the latter, condensation and charge renormalization depend on the sphere size, charge density, and salt concentration. For our CPPM parameters, close to physiological ones for globular proteins, we operate in a regime of intermediate $\kappa R \simeq 1$ and small structural charges of the globule and have not found any charge renormalization effects.[54] Hence, it is not unlikely that the counterion-release concept can only account for binding effects near the PE while ions around the patches have to be treated within a conventional ionic-screening framework.

To account for screening effects, we propose a combined CR/DH-screening approach, where we consider the explicit condensation effect only on the PE and treat the rest of the system in a simplified DH picture to include the effects of screening. The strategy is to map the simulated CPPM-PE system onto an interacting charge-multipole system and treat it on an analytic Debye-Hückel level. An illustrating sketch is shown in Fig. 3. In our discussion later, we will revolve around the one-patched, dipolar P^1_{12} type of CPPM. In our simplified model, therefore, the CPPM has a radius $R_P = 2.0$ nm and a negative charge $Q_P = Z_P e = -20e$ located in its center, while a point charge with valence $s = +12$, representing the positive patch, is located on the surface along the connecting axis. The PE chain is modeled as a charged sphere with effective charge $Q_{PE} = Z_{PE}e$ and effective radius R_{PE}. For such a simplified model, where an extended dipole within a globule (CPPM) interacts with a monopolar blob (PE), the electrostatic association free energy at contact of the two spheres ($r_{min} = R_P + R_{PE}$) can be written down on a Debye-Hückel level as

$$\begin{aligned}\beta w_{min}(c_s) = &\frac{Z_P Z_{PE}\lambda_B}{(R_P + R_{PE})[1+\kappa(c_s)R_P][1+\kappa(c_s)R_{PE}]} \\ &+ \frac{s Z_{PE}\lambda_B}{R_{PE}[1+\kappa(c_s)R_{PE}]} + N'\ln(c_s/c_{PE}),\end{aligned} \tag{10}$$

where the first term accounts for screened monopole charge repulsion and the second term effectively describes the screened electrostatic patch-PE attraction, and $\kappa(c_s) = \sqrt{8\pi\lambda_B c_s}$ is the usual inverse DH screening length. The last term is the contribution from the released ions from the PE chain according to the Record/Lohman approach in Eq. (8). The effective charge of the PE chain will be taken from the simulations in which the number of condensed counterions is explicitly calculated. The remaining free parameter R_{PE} will be fitted to the results from the simulations of the "real" CPPM-PE complex and is expected to be on the order of the radius of gyration of the chain of nanometer size. Note again that the contribution of the configurational rearrangements of the PE on the extended patch surface is not considered in this model, but believed to be small (on the order of one k_BT) with respect to the calculated binding affinities in the tens of k_BT.

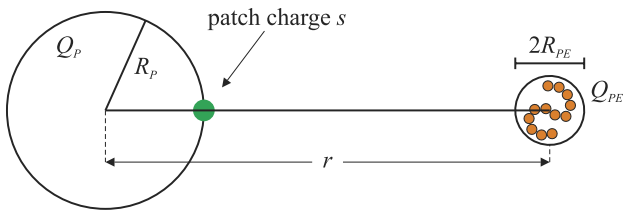

FIG. 3. Simple electrostatic model for describing the salt concentration dependence of the binding free energy of a CPPM-PE complex. The PE chain on the right-hand-side is modeled as a charged sphere with effective charge Q_{PE} and effective radius R_{PE}. The simplified CPPM (left-hand-side) has a radius R_P and a negative charge Q_P located in its center, while a point charge with valence s (green spot), representing the positive patch, is located on the surface along the connecting axis.

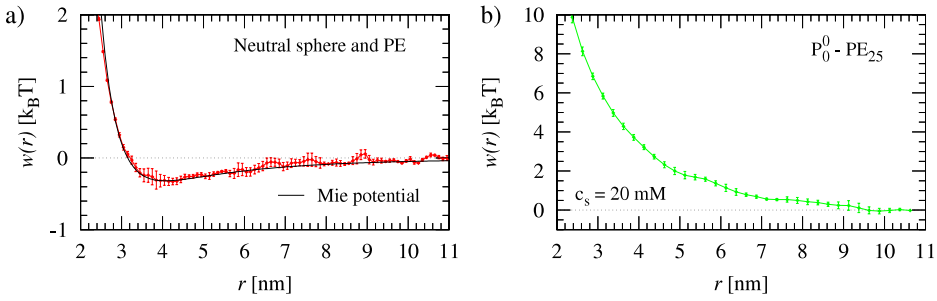

FIG. 4. (a) Simulated PMF between a fully neutral spherical globule (no beads charged) and a neutral PE_{25}. The solid line represents a fit by the Mie potential Eq. (4). (b) PMF of a charged P_0^0-PE_{25} complex in an ionic solution of c_s = 20 mM.

IV. RESULTS

A. Reference cases

We start our discussion of the PMFs with two reference cases specified by, first, a charge-free system which consist only of a neutral sphere and a short neutral PE_{25}, see Fig. 4(a), and, second, the rather homogeneously charged CPPM P_0^0 and the charged PE_{25} in an explicit ionic solution, see Fig. 4(b). Note again that the PMF is plotted versus the distance between the centers of mass of both macromolecules. The PMF of the neutral complex features a weak but long-ranged attraction but is otherwise repulsive for short distances. The solid black line represents the Mie potential. It was used to fit the PMF with $n = 5, m = 3, \sigma^* = 3.15$ nm, $\epsilon^* = 0.33$ k_BT, and $R_0 = 2.05$ nm and showed good conformity. The attraction must be assigned to vdW interactions (modeled by the LJ interaction between all beads), while the repulsion at short separations is due to the entropic penalty from restricted chain (excluded-volume) configurations of the PE that has to obey to the constraint of a close center-of-mass distance. As expected, the simulated PMF of the charged P_0^0-PE_{25} complexation at $c_s = 20$ mM in Fig. 4(b) is purely repulsive due to monopolar charge repulsion. We will now investigate the effect of changing the CPPM charge distributions on the effective interaction in more detail.

B. Results for one-patched CPPMs

The results of CPPM-PE_{25} simulations with one patch, P_s^1, and growing patch charge $s = 8, 12, 16$ at 20 mM salt concentration are shown in Fig. 5, respectively. The PMFs are now strongly attractive in the tens of k_BT for a wide distance range apart from a small repulsive barrier at around $r \simeq 6$ nm. As argued by Wu *et al.*,[37] attractive electrostatic forces between domains of opposite charges outweigh the repulsion between the domains carrying charges of equal sign. For rising patch charge s (and thus increasing dipole) of the CPPM, the attraction is more pronounced and the barrier vanishes. The insets in Table II show typical configurations of the CPPM-PE complex in the stable bound state at $r \simeq 2.5$ nm. Here, we can see that almost the entire chain is adsorbed on the patch. Configurations for other distances are also displayed in Table II. For $r \simeq 10$ nm, the PE is desorbed and exhibits relatively stiff, rod-like configurations. For a closer distance of about $r \simeq 6$ nm,

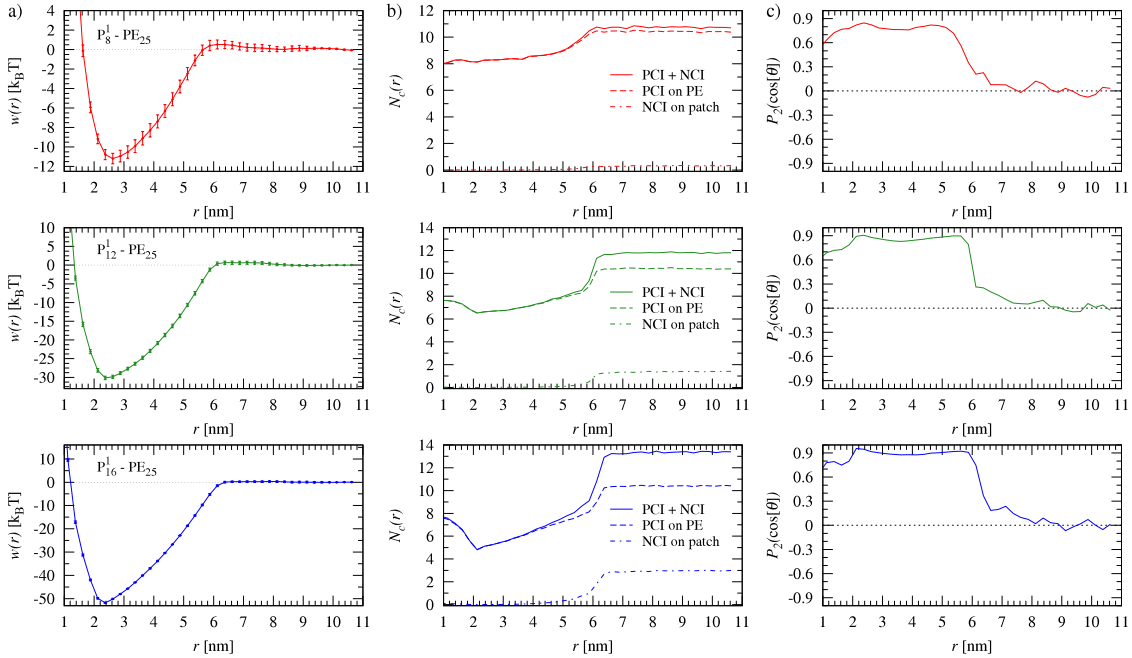

FIG. 5. Simulation results of P_s^1-PE_{25} complexes with $s = 8, 12, 16$ in an electrolyte concentration of $c_s = 20$ mM. (a) PMF as a function of the distance r of the centers of mass of the CPPM and PE. (b) Number of condensed ions $N_C(r)$ as a function of r. PCI denotes the number of positively charged ions condensed on the PE and NCI is the number of negatively charged ions condensed on the CPPM patch. (c) Patch orientation with respect to the mass centers of the CPPM and PE.

TABLE II. Snapshots of various CPPM-PE complexes at $c_s = 20$ mM and different distances r. The green colored beads are positively charged ions while the red colored beads are negative ions.

Label \ r (nm)	∼1.5	∼2.5	∼5–6	∼10
P_8^1-PE_{25}				
P_{12}^1-PE_{25}				
P_{16}^1-PE_{25}			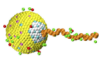	
P_8^2-PE_{25}				
P_{12}^2-PE_{25}			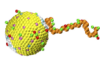	

the PE is able to reach out and touch the attractive patch; this is reflected by the onset of attraction in the PMFs in Fig. 5. The distance $r \simeq 1.5$ nm in Table II corresponds to the closest distance approachable in our steered simulations and is energetically strongly penalized. Here, the PE embraces the CPPM to fulfil the external force constraint in the simulation that the PE center of mass has to be close to that of the CPPM.

The number of negatively charged ions (NCIs) as well as positively charged ions (PCIs) condensed on the CPPM patch and on the PE for the P_s^1 simulations are shown in Fig. 5(b). At large separations, the number of condensed ions is fairly constant while the absolute value increases with growing patch charge s. When the PE begins to adsorb on the patch, $r \lesssim 6$ nm, counter- and co-ions on both molecules are simultaneously released, their number increasing with further approach of

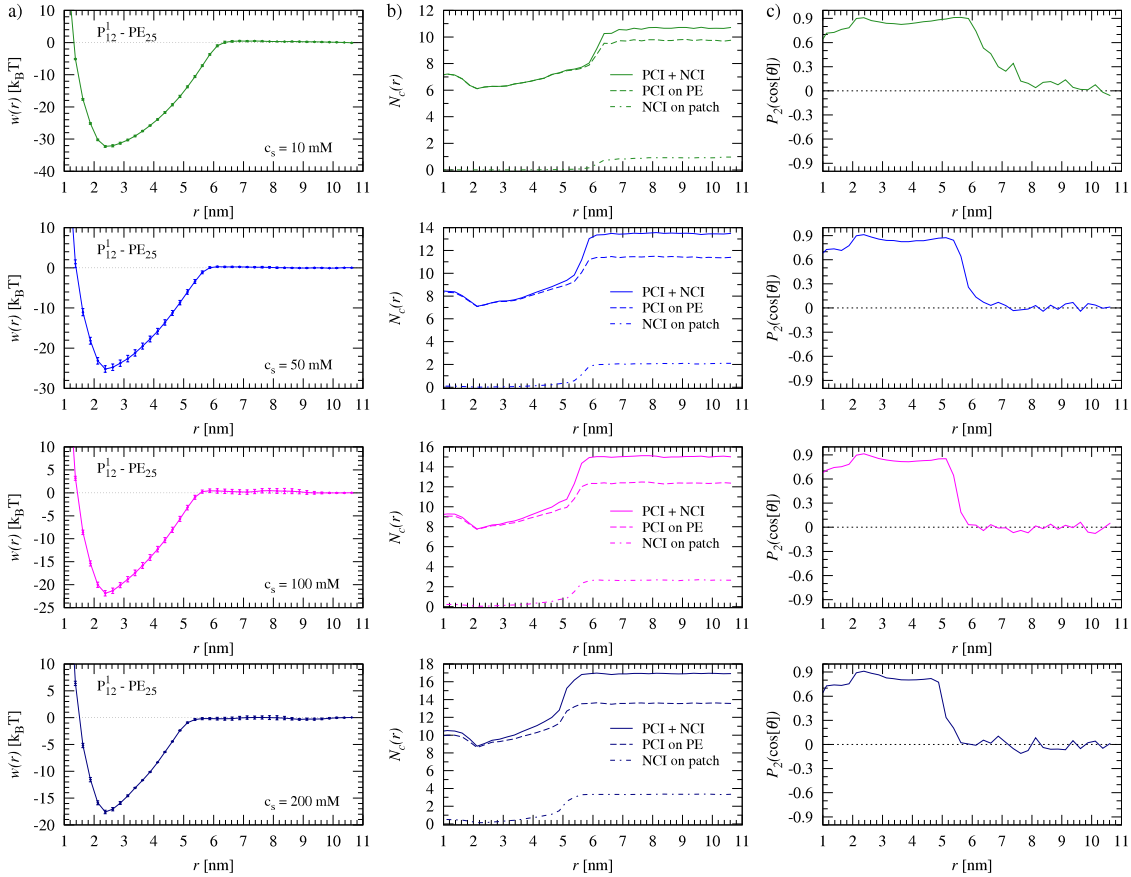

FIG. 6. Simulation of P_{12}^1-PE_{25} at different salt concentration ranging from 10 mM to 200 mM. (a) PMF as a function of the distance r of the centers of mass of the CPPM and PE. (b) Number of condensed ions $N_C(r)$ as a function of r. PCI denotes the number of positively charged ions condensed on the PE and NCI is the number of negatively charged ions condensed on the CPPM patch. (c) Patch orientation with respect to the mass centers of the CPPM and PE.

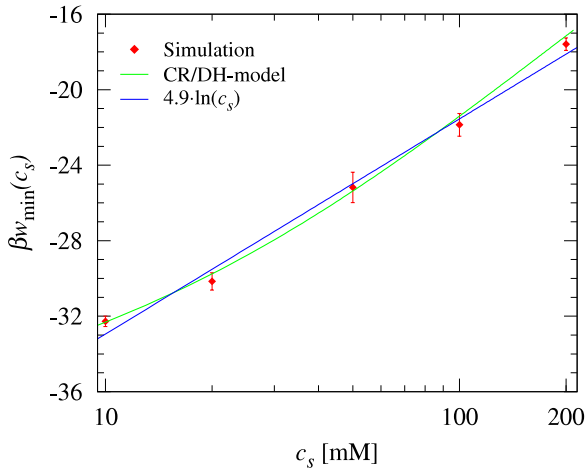

FIG. 7. The binding affinity represented by the minimum value of the PMF, $w_{\min}$, of the P^1_{12}-PE_{25} complex as a function of the salt concentration c_s (red symbols) in a lin-log plot. The linear blue solid line is a fit according to the function $a + N' \ln(c_s)$ with $a = -44.3$ and $N' = 4.9$. The green solid line is a fit to the combined CR/DH model around Eq. (10), see text for explanation.

the associating partners. Hence, CPPM-PE complexation is accompanied by a significant release of condensed ions, mostly stemming from the PE. A detailed analysis on numbers will follow in the next paragraph. In Fig. 5(c), the patch orientations along the separation r with respect to the distance vector are presented. For large distances ($r > 7$ nm), no correlation effect is observable; however, when the PE begins to attach to the patch with its first monomer, a favorite orientation of the patch towards the PE immediately locks in. This orientation persists until the PE is completely attached to the patch. For very small distances $r \lesssim 2$ nm, the orientation correlation weakens due to the (forced) embracing of the PE around the CPPM.

The influence of the ionic strength on the PMF and the ion release is systematically investigated at hand of the P^1_{12}-PE_{25} complex. The results for salt concentrations between 10 mM and 200 mM are presented in Fig. 6. First of all, it is evident that the attraction of the PMFs (Fig. 6(a)) decreases with increasing salt concentration c_s since the electrostatic interaction between the patch and the PE monomers is increasingly screened. A further effect of the screening is that the beginning of the attraction (adsorption of one of the PE head monomers to the patch) is shifted to shorter separations with increasing c_s due to a lesser stiffness of the PE chain. The corresponding number of condensed ions N_C is shown in Fig. 6(b), respectively. It is clear that increasing the ionic strength leads to more condensed ions on both molecules which can be unambiguously verified from the trajectories. The average number of released ions is between 4.4 for the lowest salt concentration and up to 7.8 for the highest salt concentration. The position of the N_C-minimum roughly coincides with the PMF minimum, that is, there is a clear correlation between ion release and attraction for all salt concentrations. The patch orientation behavior, cf. Fig. 6(c), does not exhibit any marked salt concentration behavior, apart from a shorter correlation range for increasing c_s due to the shorter attraction range discussed above.

C. Salt concentration dependence of the binding affinity

To analyze the correlation between the free energy of binding w_{min} (the "binding affinity") and salt concentration in more detail, we plot in Fig. 7 the variation of the PMF minimum with the logarithm of the salt concentration $\ln(c_s)$. As motivated by our discussion on ion release effects around Eq. (8) in Section III D, we have fitted the data with a function of the form $\beta w_{\min} = a + N' \ln(c_s)$. The result is also shown in Fig. 7. We see that it represents actually a very satisfactory fit to the data with $a = -44.3$ and $N' = 4.9$, implying that on average 4.9 ions are released upon complexation.

We go further into the details of the counterion-release analysis by actually counting ions and evaluating the free energy changes corresponding to ions released from patch and PE as defined in Eq. (9), respectively. The results are summarized in Table III. First, we would like to draw the attention to the value of N_+^{apart}, the number of condensed ions on the PE chain in the isolated state. With a Manning parameter of $\xi = 1.78$, we expect $N_{\text{mon}}(1 - 1/\xi) = 10.9$ counterions to be condensed right at the chain. As we see in Table III, we indeed find numbers between 9.7 at the lowest salt concentration up to 13.6 at the highest c_s, corroborating with the prediction but also exhibiting a noticeable salt dependence. The number of released ions from the chain upon complexation, ΔN_+, however, only slightly depends on salt, increasing from roughly 3.5 to 4.7. This also agrees well with the prediction from Manning theory that $s(1 - 1/\xi) = 5.2$ should be released from the PE upon binding of s monomers to the patch with $s = 12$ charges. Hence, the ion-PE system behaves as expected within

TABLE III. A summary of the values of the PMF minimum $w_{\min}$ with respect to the salt concentration c_s and the number of condensed ions when the CPPM and PE are apart (N_i^{apart}) and in the complexed state ($N_i^{\min}$) taken from the data for P^1_{12} in Fig. 6. The difference of condensed ions is then $\Delta N_i = N_i^{\text{apart}} - N_i^{\min}$. The concentration c_{patch} is the local density of negative ions on the CPPM patch. For c_{PE} in Eq. (9) we used a constant 3.5 M as measured in our simulations.

		Patch					PE			
c_s (mM)	$w_{\min}$ (k_BT)	N_-^{apart}	$N_-^{\min}$	ΔN_-	c_{patch} (M)	βw_{patch}	N_+^{apart}	$N_+^{\min}$	ΔN_+	βw_{PE}
10	−32.3	0.96	0.00	0.96	1.36	−4.7	9.69	6.24	3.45	−20.2
20	−30.3	1.41	0.00	1.41	1.99	−6.5	10.39	6.62	3.77	−19.4
50	−25.3	2.09	0.02	2.08	2.96	−8.5	11.35	7.22	4.12	−17.5
100	−21.9	2.65	0.05	2.60	3.75	−9.4	12.42	7.93	4.50	−16.0
200	−17.6	3.31	0.15	3.16	4.68	−10.0	13.59	8.92	4.67	−13.4

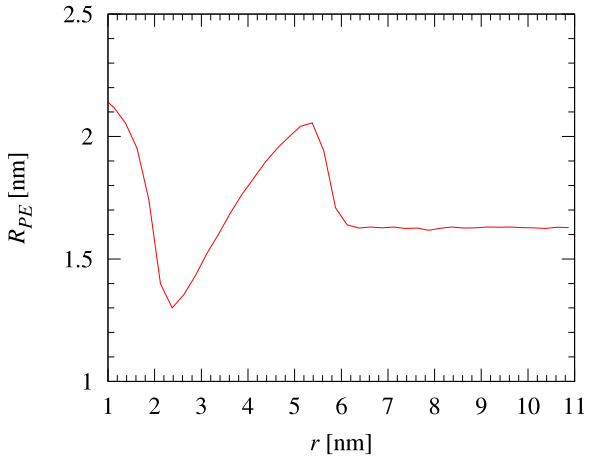

FIG. 8. The mean radius of gyration R_{PE} of the 25meric PE chain resolved versus the center-of-mass distance to the P^1_{12} CPPM at a salt concentration of 50 mM. The PE bulk value of the size, $R_{PE} \simeq 1.6$ nm, increases at intermediate distances ($r \simeq 5$ nm), where the chain stretches out, to a value of $R_{PE} \simeq 2.1$ nm and collapses to $R_{PE} \simeq 1.3$ nm in the bound state ($r \simeq 2.4$ nm). Compare also to the configurational snapshots in Table II.

the Manning-like picture and shows a robust ion-condensation and release effect.

In contrast to the ionic behavior at the PE, the number of accumulated and released ions on the CPPM patch, ΔN_-, increases from about 1 to 3.2 in the considered concentration range, i.e., a relatively strong salt concentration dependence of the number of released ions is found at the patch. The individual free energy contributions w_{patch} and w_{PE}, evaluated by Eq. (9), are also shown in Table III. Attractive contributions from the patch are actually growing (from about -5 to $-10\ k_BT$) for increasing c_s due to the significant increase of accumulated ions on the patch. In contrast, the contribution from the PE is decreasing (from about -20 to $-13\ k_BT$) because the number of condensed ions stays relatively constant. Interestingly, the sum of both contributions only shows little salt dependence and is about $-25 \pm 1\ k_BT$, while the simulated free energy increases from ca. $-32\ k_BT$ at 10 mM to ca. $-18\ k_BT$ at 200 mM. Clearly, the counterion-release approach Eq. (9) alone cannot satisfactorily describe the values and trends of the binding affinity with salt concentration. We believe that this must be assigned to a missing counterion-condensation mechanism on the CPPM patch, at which only conventional charge screening effects apparently play a role. We note that we have played around a bit with the cutoff radii that define the condensed layer around the patch in a reasonable range but have not found any qualitative improvement of the prediction.

The charge screening effect should be captured in our combined CR/DH model, Eq. (10), introduced in Section III D. A best fit is also presented in Fig. 7. Since we find on average about 8 ions still condensed on the complexed PE, the PE charge Q_{PE} was fixed by an effective valence of $-25 - (-8) = -17$. The number of condensed ions on the PE, N', was fixed to 4.9 as found in the Record-Lohman fit. The only remaining fit parameter is the effective size of the adsorbed chain, R_{PE}. For the best fit, we find $R_{PE} = 1.17$ nm. This value is indeed close to both the patch size and the mean radius of gyration of about 1.3 nm in the bound state (cf. Fig. 8, where we plot the distance-resolved radius of gyration of the PE, R_{PE}). As we can see in Fig. 7, the fit describes the simulated data very well with essentially only one fit-parameter of reasonable value. It is interesting to see that the DH part of the theory induces some curvature to the fitted curve in addition to the linear logarithmic behavior in this log-lin plot. Actually, such a curvature can also be noticed formed by the simulation data points. Hence, we have strong indications that the combined CR/DH model captures the right physics in the system, in particular, the fact that the condensed ions on the PE play the decisive role in the counterion-release framework.

D. Results for two-patched CPPMs

Let us now turn our discussion to the two-patched CPPMs. Fig. 9 shows results of CPPM-PE_{25} complexes with two ($m = 2$), antipodally aligned patches in an ionic solution of 20 mM. Despite an additional patch, the simulated PMFs between $[P^2_8/P^2_{12}]$-PE_{25} in Fig. 9(a) are less attractive as compared to P^1_s-PE_{25} systems with $s = 8, 12$, see Fig. 5(a). Furthermore, a distinct shift of the global minimum to a larger separation

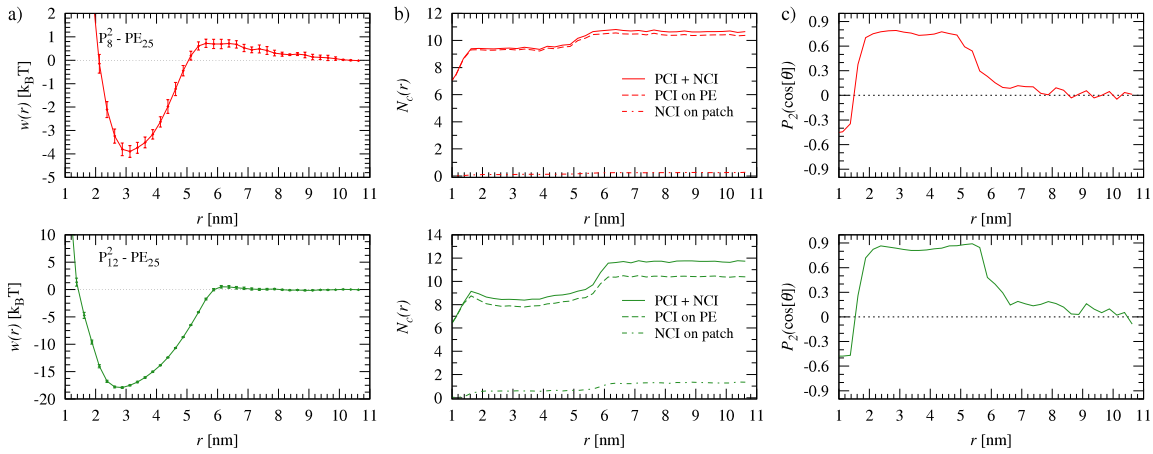

FIG. 9. Simulation results of P^2_s-PE_{25} complexes with $s = 8, 12$ at $c_s = 20$ mM. (a) PMF as a function of the distance r of the centers of mass of the CPPM and PE. (b) Number of condensed ions $N_C(r)$ as a function of r. PCI denotes the number of positively charged ions condensed on the PE and NCI is the number of negatively charged ions condensed on the CPPM patch. (c) Patch orientation with respect to the mass centers of the CPPM and PE.

is present. A possible explanation could be that in CPPMs with $m = 2$ the negative charges are denser distributed on the surface leading to a raised repulsive electrostatic interaction and a reduced attraction between PE monomers and the CPPM. By counting the condensed ions N_C on the both molecules again ion release is found, see Fig. 9(b), where ions are mainly released from the PE. As in the one-patch systems, the attraction is accompanied by a strong orientation of the interacting attractive patch to the PE, see Fig. 9(c). The orientation is reversed at very small distances $r \lesssim 1.8$ nm, but note that those are improbable to observe in equilibrium anyway due to the high free energy penalty. Hence, for the short PE_{25} chain that cannot reach to the second patch of the CPPM, the results are qualitatively similar to that of the analogous one-patch system, albeit with considerable less attraction. We will now see that a longer chain, which can interact with both patches simultaneously, will lead to qualitatively very different PMFs.

The PMFs of complexation of the two-patched CPPM with the longer chain, P^2_{12}-PE_{50}, simulated at salt concentrations ranging from $c_s = 20$ mM to $c_s = 200$ mM is presented in Fig. 10(a). In stark contrast to the shorter chain, we now observe a two-step PE adsorption to the CPPM with a second but metastable attraction minimum at $r \simeq 4.5$ nm for the smallest salt concentration, decreasing to $r \simeq 3.5$ nm for the largest salt concentration. As we see from the graphical snapshots in Table IV, the metastable minimum at $r \simeq 4.5$ nm corresponds to binding configurations where the PE is attached solely to one of the two patches. The global minimum is now shifted towards much smaller distances $r \simeq 1.5$ nm when compared to the one-patched systems and shorter chains. The corresponding binding configurations are also summarized in Table IV: by fully embracing the globule, extended parts of both the head and the tail of the chain can now simultaneously interact with both of the patches while the center-of-mass of the chain is very close to that of the globule. The global and local minima are separated by a free energy barrier at $r \simeq 2.5$–3 nm. The barrier must be assigned to the electrostatic repulsion between one of the loose ends of the PE (while the other is attached to one patch) and the negative (un-patched) parts of the globule when the PE attempts to embrace the globule to attach to the second patch. Regarding the number of released ions, we find that the two-state PMF behavior is also reflected by a two-step release of ions as shown in Fig. 10(b). The orientation of the corresponding patch vector versus distance is given in Fig. 10(c), respectively. We again observe the strong patch alignment induced by PE binding for larger separations as in the previous cases. In addition, due to the large conformational change of the complex at short separations, when crossing from the metastable PMF minimum to the global one, the orientation drastically changes from parallel alignment of patch-PE to antiparallel alignment with the PE fully embracing the globule.

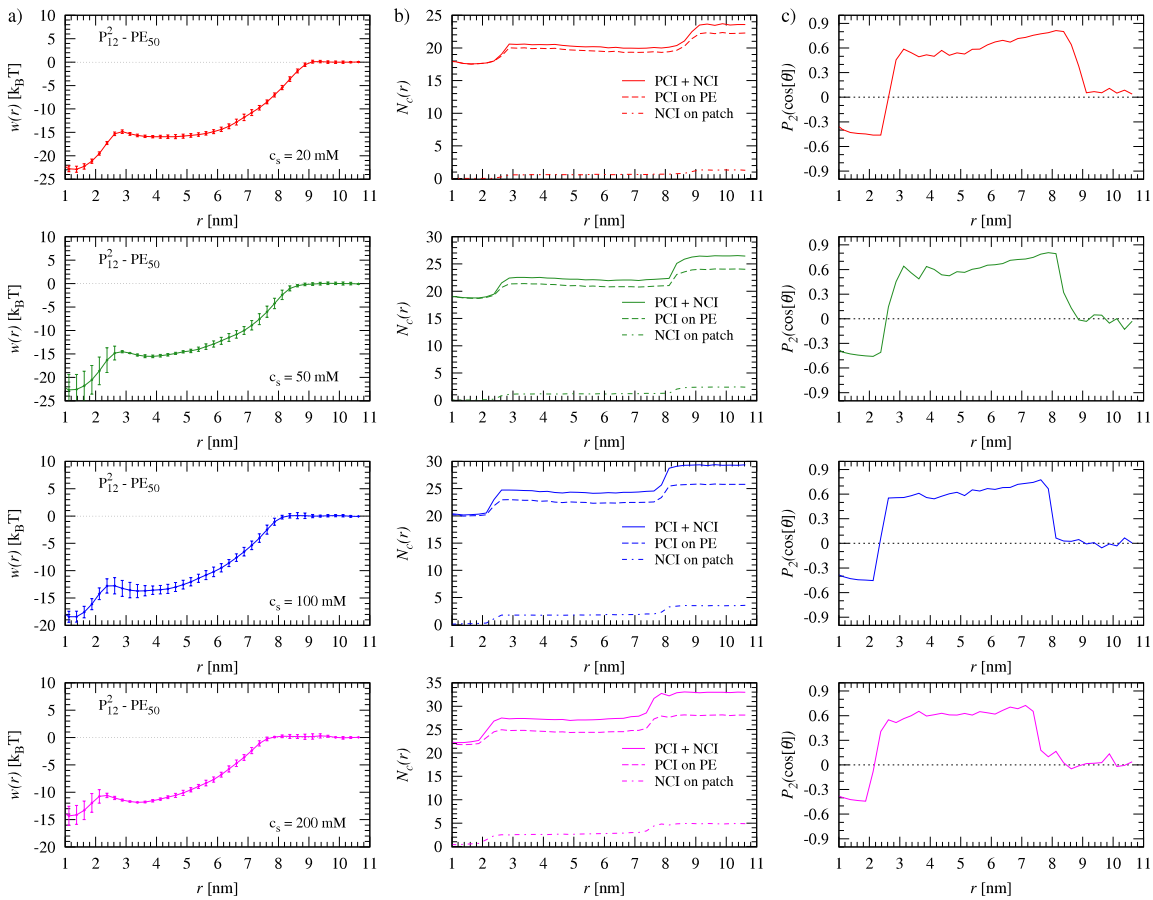

FIG. 10. Simulation results of P^2_{12}-PE_{50} complexes at various concentrations. (a) PMF as a function of the distance r of the centers of mass of the CPPM and PE. (b) Number of condensed ions $N_C(r)$ as a function of r. PCI denotes the number of positively charged ions condensed on the PE and NCI is the number of negatively charged ions condensed on the CPPM patch. (c) Patch orientation with respect to the mass centers of the CPPM and PE.

TABLE IV. Snapshots of P^2_{12}-PE_{50} complexes at various salt concentration and different distances r. The green colored beads are positively charged ions while the red colored beads are negative ions.

c_s (mM) \ r (nm)	∼1.5	∼4.5	∼7–9	∼10
20			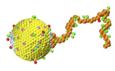	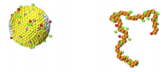
50			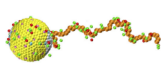	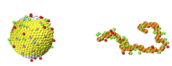
100			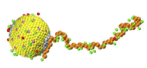	
200			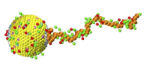	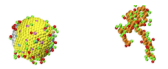

V. SUMMARY AND CONCLUDING REMARKS

In the present work, implicit solvent/explicit salt Langevin simulations have been carried out to determine the structure and interactions of relatively short and highly charged PE chains complexing with like-charged CPPMs of nanometer size. We have observed strong electrostatic attractions between the CPPM and the like-charged PE that depend on the salt concentration, patch charge, and the degree of patchiness, leading to a variety of complexation structures along the distance reaction coordinate. In particular, a novel two-state binding behavior for PEs with length comparable to the CPPM radius in case of two-patched CPPMs has been identified. Here, the PE ends are attached to the patches but the rest of the chain is repelled so that it resembles a "tea-pot handle" like structure. Our systematic analysis has further demonstrated a clear correlation between the binding affinity and the number of released ions, identifying them as a major driving factor for the strong association.

We can conclude that in general the counterion-release picture is valid and clearly dominates the interactions in our multipolar PE-patchy particle systems. As a consequence, the large binding affinities are mostly governed by the translational entropy of released ions. A quantitative analysis of the partial contributions of the number of accumulated ions released from protein patch and PE, however, appeared less simple due to somewhat ill-defined definitions of what are condensed and screening ions, in particular, in the case of the patch region. Due to the relatively large salt-concentration dependence of the ions accumulated on the protein patch, no reasonable analysis in terms of the counterion-release effect could be made for the patch. We have reconciled this mis-interpretation by a combined CR/DH model, where we considered only the release effects at the PE, which we proved to be quite robust, while the rest of the system was treated by a simplified DH screening model. The CR/DH model described the binding affinity quantitatively using only one, physically reasonable fitting parameter, corroborating that our model has captured the essential physics.

We finally note that our findings are fully supported by a recent joint experimental/simulation study of the like-charge complexation of HSA with a short PE chain.[30] In the simulation part of the latter study, the protein charge distribution was explicitly modeled and a very robust ion release-driven binding of the PE to a positively charged binding patch on the HSA was observed. Our present work should be thus useful for the interpretation of experimental structures and binding affinities found for protein or nanoparticle complexation with like-charged PE chains or for the adsorption of proteins on materials with PE coatings.

ACKNOWLEDGMENTS

The authors thank Stefano Angioletti-Uberti for inspiring discussions. The authors acknowledge funding by the Deutsche Forschungsgemeinschaft (DFG), the Alexander-von-Humboldt (AvH) foundation, the Helmholtz Virtual Institute for Multifunctional Biomaterials for Medicine, and the Helmholtz Association through the Helmholtz-Portfolio Topic "Technology and Medicine."

[1]M. Muthukumar, C. K. Ober, and E. L. Thomas, Science **277**, 1225 (1997).
[2]R. Duncan, Nat. Rev. Drug Discovery **2**, 347 (2003).
[3]D. Bontempo and H. D. Maynard, J. Am. Chem. Soc. **127**, 6508 (2005).
[4]P. Dutta, S. Tripathi, G. Mehrotra, and J. Dutta, Food Chem. **114**, 1173 (2009).
[5]S. Shu, C. Sun, X. Zhang, Z. Wu, Z. Wang, and C. Li, Acta Biomater. **6**, 210 (2010).
[6]A. Marin, D. P. DeCollibus, and A. K. Andrianov, Biomacromolecules **11**, 2268 (2010).
[7]H. Zhang, A. Saiani, J.-M. Guenet, and R. Curtis, Macromol. Symp. **251**, 25 (2007).
[8]C. Cooper, P. Dubin, A. Kayitmazer, and S. Turksen, Curr. Opin. Colloid Interface Sci. **10**, 52 (2005).
[9]A. B. Kayitmazer, D. Seeman, B. B. Minsky, P. L. Dubin, and Y. Xu, Soft Matter **9**, 2553 (2013).
[10]F. W. Wiegel, J. Phys. A: Math. Gen. **10**, 299 (1977).
[11]T. Odijk, Macromolecules **23**, 1875 (1990).
[12]F. von Goeler and M. Muthukumar, J. Chem. Phys. **100**, 7796 (1994).
[13]R. R. Netz and J.-F. Joanny, Macromolecules **32**, 9026 (1999).
[14]K.-K. Kunze and R. R. Netz, Phys. Rev. Lett. **85**, 4389 (2000).
[15]R. de Vries, F. Weinbreck, and C. G. de Kruif, J. Chem. Phys. **118**, 4649 (2003).
[16]C. Y. Kong and M. Muthukumar, J. Chem. Phys. **109**, 1522 (1998).
[17]T. Nguyen and B. Shklovskii, Phys. A **293**, 324 (2001).
[18]F. Carlsson, P. Linse, and M. Malmsten, J. Phys. Chem. B **105**, 9040 (2001).
[19]P. Chodanowski and S. Stoll, J. Chem. Phys. **115**, 4951 (2001).
[20]M. Jonsson and P. Linse, J. Chem. Phys. **115**, 10975 (2001).
[21]R. Messina, C. Holm, and K. Kremer, J. Chem. Phys. **117**, 2947 (2002).
[22]J. Dzubiella, A. G. Moreira, and P. A. Pincus, Macromolecules **36**, 1741 (2003).

[23]R. Messina, C. Holm, and K. Kremer, Langmuir **19**, 4473 (2003).
[24]R. de Vries, J. Chem. Phys. **120**, 3475 (2004).
[25]F. L. B. da Silva, M. Lund, B. Jönsson, and T. Åkesson, J. Phys. Chem. B **110**, 4459 (2006).
[26]F. L. B. da Silva and B. Jönsson, Soft Matter **5**, 2862 (2009).
[27]D. Truzzolillo, F. Bordi, F. Sciortino, and S. Sennato, J. Chem. Phys. **133**, 024901 (2010).
[28]G. Luque-Caballero, A. Martín-Molina, and M. Quesada-Pérez, J. Chem. Phys. **140**, 174701 (2014).
[29]S. J. de Carvalho, R. Metzler, and A. G. Cherstvy, Phys. Chem. Chem. Phys. **16**, 15539 (2014).
[30]S. Yu, X. Xu, C. Yigit, M. van der Giet, W. Zidek, J. Jankowski, J. Dzubiella, and M. Ballauff, Soft Matter **11**, 4630 (2015).
[31]J. M. Park, B. B. Muhoberac, P. L. Dubin, and J. Xia, Macromolecules **25**, 290 (1992).
[32]T. Hattori, R. Hallberg, and P. L. Dubin, Langmuir **16**, 9738 (2000).
[33]E. Seyrek, P. L. Dubin, C. Tribet, and E. A. Gamble, Biomacromolecules **4**, 273 (2003).
[34]K. W. Mattison, P. L. Dubin, and I. J. Brittain, J. Phys. Chem. B **102**, 3820 (1998).
[35]A. Diehl, H. A. Carmona, and Y. Levin, Phys. Rev. E **64**, 011804 (2001).
[36]T. E. Angelini, H. Liang, W. Wriggers, and G. C. L. Wong, Proc. Natl. Acad. Sci. U. S. A. **100**, 8634 (2003).
[37]J. Wu, D. Bratko, H. W. Blanch, and J. M. Prausnitz, Phys. Rev. E **62**, 5273 (2000).
[38]R. K. Hallberg and P. L. Dubin, J. Phys. Chem. B **102**, 8629 (1998).
[39]B. Ball *et al.*, J. Phys. Chem. B **106**, 2357 (2002).
[40]C. G. de Kruif, F. Weinbreck, and R. de Vries, Curr. Opin. Colloid Interface Sci. **9**, 340 (2004).
[41]C. Czeslik, G. Jackler, R. Steitz, and H. H. von Grunber, J. Phys. Chem. B **108**, 13395 (2004).
[42]S. Rosenfeldt, A. Wittemann, M. Ballauff, E. Breininger, J. Bolze, and N. Dingenouts, Phys. Rev. E **70**, 061403 (2004).
[43]J. Gummel, F. Cousin, and F. Boué, J. Am. Chem. Soc. **129**, 5806 (2007).
[44]K. Henzler, B. Haupt, K. Lauterbach, A. Wittemann, O. Borisov, and M. Ballauff, J. Am. Chem. Soc. **132**, 3159 (2010).
[45]A. V. Dobrynin and M. Rubinstein, Prog. Polym. Sci. **30**, 1049 (2005).
[46]R. M. Fuoss, A. Katchalsky, and S. Lifson, Proc. Natl. Acad. Sci. U. S. A. **37**, 579 (1951).
[47]G. S. Manning, J. Chem. Phys. **51**, 924 (1969).
[48]F. Oosawa, *Polyelectrolytes* (Marcel Dekker, New York, 1971).
[49]M. T. Record, Jr., T. M. Lohman, and P. D. Haseth, J. Mol. Biol. **107**, 145 (1976).
[50]L. Belloni, Colloids Surf., A **140**, 227 (1998).
[51]R. R. Netz and H. Orland, Eur. Phys. J. E: Soft Matter **11**, 301 (2003).
[52]G. S. Manning, J. Phys. Chem. B **111**, 8554 (2007).
[53]Z. Ou and M. Muthukumar, J. Chem. Phys. **124**, 154902 (2006).
[54]C. Yigit, J. Heyda, and J. Dzubiella, J. Chem. Phys. **143**, 064904 (2015).
[55]V. N. Uversky, Biochemistry **32**, 13288 (1993).
[56]H. M. Berman *et al.*, Nucleic Acids Res. **28**, 235 (2000).
[57]J. D. Ferry and J. L. Oncley, J. Am. Chem. Soc. **63**, 272 (1941).
[58]E. Pezron, L. Leibler, and F. Lafuma, Macromolecules **22**, 2656 (1989).
[59]J.-L. Popot, E. A. Berry, D. Charvolin, C. Creuzenet, C. Ebel, D. M. Engelman, M. Flötenmeyer, F. Giusti, Y. Gohon, P. Hervé, Q. Hong, J. H. Lakey, K. Leonard, H. A. Shuman, P. Timmins, D. E. Warschawski, F. Zito, M. Zoonens, B. Pucci, and C. Tribet, Cell. Mol. Life Sci. CMLS **60**, 1559 (2003).
[60]F. Wiesbrock, R. Hoogenboom, M. A. M. Leenen, M. A. R. Meier, and U. S. Schubert, Macromolecules **38**, 5025 (2005).
[61]B. Hess, C. Kutzner, D. van der Spoel, and E. Lindahl, J. Chem. Theory Comput. **4**, 435 (2008).
[62]U. Essmann, L. Perera, M. L. Berkowitz, T. Darden, H. Lee, and L. G. Pedersen, J. Chem. Phys. **103**, 8577 (1995).
[63]B. Israelewitz, J. Baudry, J. Gullingsrud, D. Kosztin, and K. Schulten, J. Mol. Graphics Modell. **19**, 13 (2001).
[64]R. M. Neumann, Am. J. Phys. **48**, 354 (1980).
[65]B. Hess, C. Holm, and N. van der Vegt, J. Chem. Phys. **124**, 164509 (2006).
[66]I. Kalcher and J. Dzubiella, J. Chem. Phys. **130**, 134507 (2009).
[67]M. Deserno, C. Holm, and S. May, Macromolecules **33**, 199 (2000).